Available online at www.sciencedirect.com
SCIENCE DIRECT®
Solid State Ionics 166 (2004) 365–373
SOLID STATE IONICS
www.elsevier.com/locate/ssi

Molecular dynamics simulation of lithium diffusion in $Li_2O–Al_2O_3–SiO_2$ glasses

Weiqun Li, Stephen H. Garofalini*

Department of Ceramic and Materials Engineering, Interfacial Molecular Science Laboratory, Rutgers University, 607 Taylor Road, Piscataway, NJ 08854, USA

Received 7 May 2003; received in revised form 13 November 2003; accepted 18 November 2003

Abstract

The molecular dynamics (MD) computer simulation technique has been used to study the structure of lithium aluminosilicate (LAS) glasses and the diffusion of lithium ions. Five kinds of lithium aluminosilicate glasses with different *R* (ratio of the concentration of Al to Li) values are simulated. The structural features of the simulated glasses are analyzed using Radial Distribution Functions (RDFs) and Pair Distribution Functions (PDFs). With the increase of *R*, the environments of the Li ions alter from bonding to non-bridging oxygen to bonding to the bridging oxygen associated with tetrahedral Al. The diffusion coefficients and activation energy of lithium ion diffusion in simulated lithium aluminosilicate glasses were calculated and the values are consistent with those in experimental glasses. When *R* equals 1.00, lithium ions have the lowest activation energy for diffusion. The relationship between the activation energy for lithium diffusion and the composition of these glasses is similar to that previously observed for sodium in sodium aluminosilicate glasses.

PACS: Diffusion 66.10-x; Glass 81.05-Kf; Li-ion batteries 82.47-Aa
Keywords: Glass; Lithium diffusion; Molecular dynamics

1. Introduction

In recent years, much work and research activity have been devoted to the study of solid state lithium batteries and electrochromic devices employing solid glass electrolytes as electrolytic layers [1–4]. While liquid electrolytes and polymer electrolytes offer fast transport paths for Li ion diffusion between electrodes, reactions at electrode surfaces can be detrimental. In addition, environmental effects can degrade polymer electrolytes in electrochromic devices. Thin film solid state batteries using oxide glass electrolytes have been shown to be successful [5]. In addition, such oxide glasses can be used as thin separation films between more reactive polymer electrolytes and electrodes. Thus, the oxide electrolyte has certain potential applications in thin film batteries and electrochromic devices. However, Li ion diffusion is slower in these glasses than in other electrolytes and increasing Li diffusion would be beneficial. Lithium aluminosilicate (LAS) glasses have been studied as ion conducting glasses and glass-ceramics [6–9]. The studies in those materials were often conducted on the two limits of glassy and crystalline materials with the same composition. The mechanism of Li^+ ion motion in crystalline and glassy lithium aluminosilicate with the β-eucryptite composition ($LiAlSiO_4$) was studied using a combination of structural (vibration spectroscopy, X-ray diffraction) and transport (ionic conductivity) methods by Pechenik et al. [6]. They found that the rigidly alternating potential for Li^+ ions in crystalline $LiAlSiO_4$ is substantially altered by the disorder present in the glass. This disorder strongly reduces correlation effects on ionic motion in the glass as opposed to the crystal and results in a smaller activation energy for diffusivity in the glassy $LiAlSiO_4$. A number of other experimental studies of Li diffusion in glasses have been presented, all with similar results for the activation energy of Li in oxide glasses [10–14]. As an analog to lithium silicate glasses, sodium silicate glasses show enhanced Na diffusion as a function of alumina concentration [15–20]. There are few studies on the atomic scale regarding the relationship between the glass structure, Li^+ transport properties and the composition of lithium aluminosilicate glasses. In this paper, we will focus on a computational

* Corresponding author. Tel.: +1-732-445-2216; fax: +1-732-445-3258.
E-mail address: shg@glass.rutgers.edu (S.H. Garofalini).

0167-2738/$ - see front matter © 2004 Elsevier B.V. All rights reserved.
doi:10.1016/j.ssi.2003.11.015

approach, molecular dynamics (MD) simulations, to study both the atomic scale structure and ion migration in lithium aluminosilicate glasses.

2. Computational procedure

2.1. The potential energy

In this paper, the total potential energy acting on each atom in the system was composed of contributions from two- and three-body interactions, given as:

$$V_{\text{total}} = \sum_i \sum_{j>i} V_{ij}^{(2)} + \sum_i \sum_{j\neq i} \sum_{k>j} V_{jik}^{(3)} \quad (1)$$

The two-body term is given as:

$$V_{ij}^{(2)} = A_{ij}\exp\left(\frac{-r_{ij}}{\rho_{ij}}\right) + \frac{1}{r_{ij}} q_i q_j \xi\left(\frac{r_{ij}}{\beta_{ij}}\right) \quad (2)$$

where r_{ij} is the separation distance between ions i and j, ρ_{ij} is a softness parameter (and is equal to 0.029 nm for all i, j pairs), q is the ion charge, and ξ is the complementary error function *erfc*. A_{ij} and β_{ij} depend on the ion pairs, i and j, and have been discussed previously [21–23]. The ξ function is a screening function that also reduces the formal charges on the ions as a function of ion pairs and distance.

The three-body potential is a minimum at the equilibrium angle of a three body triplet and raises the energy of the system when the angles between the partially covalently bonded species deviate from the preferred angle. This potential is applied to Si, Al, and O as central ions, i, and their first-neighbors, j and k, as triplets jik and is defined as:

$$V_{jik}^{(3)} = \lambda_{jik}\exp\left(\frac{\gamma_{ij}}{r_{ij} - r_{ij}^0} + \frac{\gamma_{ik}}{r_{ik} - r_{ik}^0}\right)\Omega_{jik} \quad (3)$$

when $r_{ij} < r_{ij}^0$ and $r_{ik} < r_{ik}^0$, and

$$V_{jik}^{(3)} = 0 \quad (4)$$

otherwise.

Table 1
Potential parameters of the two-body terms

Two-body BMH parameters, atom pair $ij=ji$	A_{ij} (fJ)	β_{ij} (nm)
Si–O	0.2962	0.234
Al–O	0.2750	0.234
Li–O	0.1300	0.240
O–O	0.3200	0.234
Si–Si	0.1877	0.230
Al–Si	0.2523	0.233
Li–Si	0.0817	0.230
Al–Al	0.3418	0.235
Li–Al	0.0817	0.230
Li–Li	0.2300	0.230

ρ_{ij} = 0.029 nm for all ij pairs.

Table 2
Three-body parameters

	r^0 (nm)	λ (10^{-18}J)	γ (nm)
X–O–X[a]	0.26	1.0	0.20
O–Si–O	0.30	24.0	0.28
O–Al–O	0.30	24.0	0.28

[a] X = Si, Al, Li.

The λ and γ are fitted parameters and r^0 is the cutoff distance to be considered for a three-body contribution. The angular part, Ω_{jik}, is given by

$$\Omega_{jik} = (\cos\theta_{jik} + \cos\theta_{jik}^0)^2 \quad (5)$$

for Si/Al/Li–O–Si/Al/Li and O–Si–O, and

$$\Omega_{jik} = [(\cos\theta_{jik} + \cos\theta_{jik}^0)\sin\theta_{jik}\cos\theta_{jik}]^2 \quad (6)$$

for O–Al–O; where θ_{jik} is the angle formed by the ions j, i, and k, with the ion i at the vertex and θ_{jik}^0 is the tetrahedral equilibrium angle of 109.4°. The three-body term is relatively weak but has been shown to help remove the overcoordinated defect species in amorphous silica [23]. Nonetheless, overcoordinated species, while less stable, are able to form as reaction intermediates, such as the trigonal bipyramidal Si in water–silica reactions or polymerization of silicic acid molecules [24–26]. The three body potential reproduces stable crystalline α-Al_2O_3 and γ-Al_2O_3 [27]; Al is six coordinated in the former and both four and six coordinated in the latter. In silicate glasses, Al is four coordinated and has been discussed with respect to simulations previously [15].

Additional details regarding the combined two- and three-body potential are described in prior work [15,23–28]. Tables 1 and 2 list all the potential parameters used in this paper.

Five bulk lithium aluminosilicate glasses with different R values were studied, where R equals the ratio of the mole concentration of Al to the mole concentration of Li, [Al]/[Li], given in Table 3. The glasses were formed using the MD melt-quench technique that involved scaling the kinetic energy of the system of atoms from elevated temperatures to 300 K through intermediate temperatures. Different quench procedures (from different elevated temperatures to room temperature) were used for the different glasses because of the compositional effects on viscosity and relaxation. The systems were all cooled to room temperature in order to perform the structural analysis of the glasses, which included determination of the radial distribution functions (RDF) and pair distribution functions (PDF). The former is summed over all ion pairs while the latter is summed over only specific ion pairs, both being time and number averaged. All bulk simulations were performed with a time step of integration of 1.0 fs in the melt-quench process, except near the glass transition temperature where a time step of integration of 0.2 fs was used to more accurately simulate

Table 3
Glass compositions, number of atoms from each species, density, and coefficient of thermal expansion (the last two columns from experimental data [37])

R-value	Glass composition	Number of atoms					Density [37] (g/cm^3)	CTE [37] (10^{-7} K^{-1})
		Si	O	Al	Li	Total		
1.50	$0.20Li_2O,0.30Al_2O_3,0.50SiO_2$	490	2058	588	392	3528	2.452	72.8
1.00	$0.25Li_2O,0.25Al_2O_3,0.50SiO_2$	500	2000	500	500	3500	2.363	78.1
0.67	$0.30Li_2O,0.20Al_2O_3,0.50SiO_2$	515	1957	412	618	3502	2.423	100.3
0.25	$0.40Li_2O,0.10Al_2O_3,0.50SiO_2$	550	1870	220	880	3520	2.381	107.4
0.00	$0.50Li_2O,0.50SiO_2$	584	1752	0	1168	3504	2.323	120

structural formation of the glasses. Periodic boundary conditions were used in the *x*, *y*, and *z* directions in these NVE simulations. The room temperature density was taken from experimental values and the volume at elevated temperatures was dependent on the experimental thermal expansion coefficient, both given in Table 3.

For diffusion analysis, each of the simulated glasses was heated from 300 to 1000, 1400, 1800, 2200, 2600, 3000, 4000, 5000, 6000 and 7000 K for 100 ps at each temperature. The simulations at the higher temperatures were used to estimate a functional 'glass transition temperature', Tg, within the timeframe of the simulations. For the purposes of these simulations, this 'Tg' was defined here as the temperature at which the diffusion coefficients of network former atoms, Si, O, and Al, are about 10^{-7}–10^{-6} cm^2/s. This was done to estimate the temperature at which network forming ions would show significant relaxation. Hence, Li ion diffusion was evaluated at lower temperatures to simulate Li ion diffusion within a matrix of nondiffusing network forming ions (Si, O, and Al). Such Li diffusion would be more consistent with Li diffusion in thin film electrolytes where the matrix structure remains predominantly in place. During the first 10 ps of all runs the temperature was kept constant by velocity rescaling every 10th time step. A time step of 0.25 fs was used in this diffusional analysis and all atom positions and velocities were saved every 0.25 ps, giving a total of 400 configurations for each glass at each temperature.

Diffusion was analyzed over the final 90 ps at each temperature, i.e. the final 360 configurations of each run. The mean square displacement (MSD), $\overline{r_\tau^2}$, averaged over all atoms in each species, N_s, is given as $\frac{1}{N_s}\sum_i^{N_s}[r_i(\tau) - r_i(t_0)]^2$, where $\tau = t_0 + \Delta t$. The MSD was averaged over 17 initial times, t_0, separated by 2.5 ps. Δt was taken for all subsequent configurations up to a total of 50 ps from each t_0. This was done for each atom type. The diffusion coefficient was then calculated from $\overline{r_\tau^2}$ as a function of τ in the long time limit,

$$D = \frac{1}{6}\left(\frac{\mathrm{d}}{\mathrm{d}\tau}\overline{r_\tau^2}\right) \tag{7}$$

Well below Tg, the network structure is essentially unchanged, with the network ions only vibrating, so the pathways for the alkali ion migration are fixed. However, the temperature was sufficiently high to enable Li diffusion. Doing this at a number of different temperatures yields an Arrhenius plot, from which it is possible to derive the activation energy for diffusion. To maintain a constant temperature during the calculation of diffusion after the initial 10 ps of temperature equilibration, the velocities of the ions were rescaled whenever the system temperature

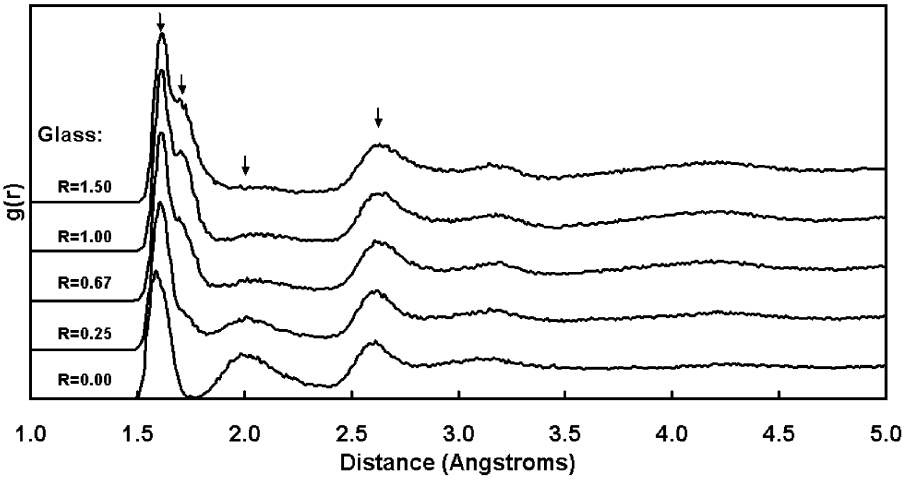

Fig. 1. Radial distribution functions (RDF) of the glasses, summed over all ions at room temperature; data displaced in *Y*-axis.

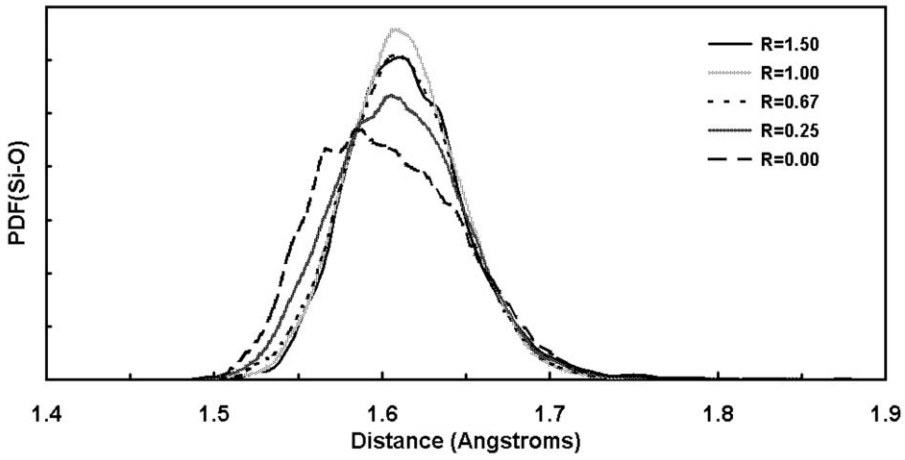

Fig. 2. The first neighbor peak in the pair distribution functions (PDF) of Si–O atom pairs at room temperature.

deviated from the desired temperature of the run by more than 100 K. Activation energies for diffusion, E^*, and diffusivity pre-exponential factors, D_0, were calculated using regression analysis of D as a function of reciprocal temperature, $1/T$.

$$D = D_0 \exp\left(\frac{-E*}{RT}\right) \tag{8}$$

3. Results and discussion

3.1. Structure

Fig. 1 shows the calculated RDFs from the models obtained by these MD simulations. The first peak near 1.60 Å, which corresponds to the first peak of the PDF of Si–O in Fig. 2, is attributed to the nearest neighboring Si–O atom pairs. The Si–O PDF (Fig. 2) clearly shows a shift to smaller bond lengths when the Li concentration exceeds that of Al. This is caused by the large concentration of non-bridging oxygens (NBO) associated with the Si as Si–O–Li in such glasses. With the increase of Al atoms in the glasses, a shoulder occurs around 1.70 Å in Fig. 1, which corresponds to the first peak of PDF of Al–O, as shown in Fig. 3, and is attributed to the nearest neighboring Al–O pairs. Similarly in Fig. 1, the third peak near 2.05 Å and the fourth peak near 2.65 Å are attributed to the nearest neighboring Li–O and O–O atom pairs, respectively, according to the result of the PDF of Li–O and O–O atom pairs shown in Figs. 4 and 5. These first neighbor distances are in good agreement with the neutron diffraction data [29] and previous simulation results [30].

Fig. 6 shows the PDF of Li–Li pairs at 300 K for several simulated glasses. The information on lithium distribution in the glasses can be obtained by analyzing the height and position of nearest neighbor peaks of Li–Li pairs. The decrease in the height of the nearest neighbor peak with the increase in R can be attributed to the decrease in Li

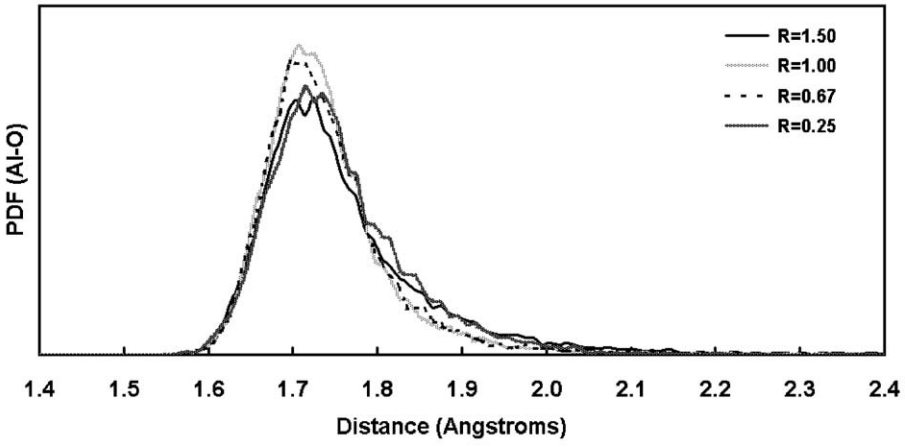

Fig. 3. The first neighbor peaks in PDF of Al–O atom pairs at room temperature.

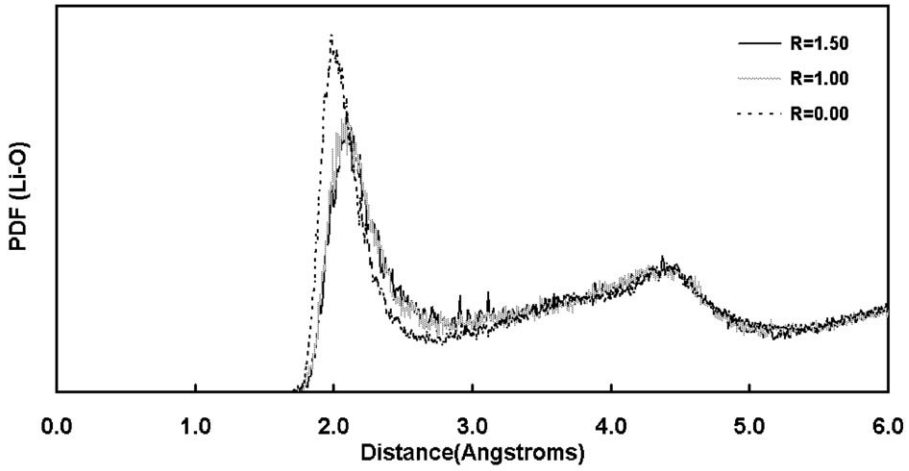

Fig. 4. PDF of Li–O atom pairs at room temperature.

concentration. Fig. 6 also shows that the position of the nearest neighbor pick shifts from 2.6 to ~ 3.0 Å with the increase of R from 0.00 to 1.50. This shift is due to the addition of Al, which decreases the number of non-bridging oxygen to which the lithium bond and generates new [AlO_4] tetrahedral sites (and the associated BO) to which lithium ions can locate. When $R \geq 1.00$, there are almost no NBOs in the glasses. Therefore, in Fig. 6, the Li–Li nearest neighbor peak in the glasses with $R = 1.00$ and $R = 1.50$ lies at the similar position of ~ 3.0 Å. This is consistent with the result of the PDF of Li–O atom pairs shown in Fig. 4. The PDF of Li–O atom pairs in $R = 1.00$ glasses is nearly identical with that in $R = 1.50$ glasses. The nearest neighbor peak of Li–O atom pairs in $R = 0.00$ glasses (corresponding to the bond length of Li–NBO) is less than that in $R = 1.00$ and $R = 1.50$ glasses (corresponding to the relative distance of Li ion with the BO between tetrahedra). The difference in X–NBO versus X–BO, where X is an alkali ion, is consistent with previous interpretations of EXAFS data [31,32] and ab initio calculations [33].

3.2. Diffusion

Fig. 7 shows an example of the mean squared displacement of the lithium ions plotted versus time for a glass with $R = 0.25$ at temperatures of 1400, 1800, 2200, 2600, and 3000 K. These temperatures correspond to approximately 0.35Tg, 0.45Tg, 0.55Tg, 0.65Tg, and 0.75Tg, where Tg, as defined in this paper, had a value of approximately 4000 K for the simulated glasses. The slopes of the curves in Fig. 7 were used in determining the diffusion coefficients for lithium ions at different temperatures via Eq. (7) for $R = 0.25$ glasses. The same method was used to calculate the lithium ion diffusion coefficients in the other four glasses with $R = 0.00$, 0.67, 1.00 and 1.50.

Fig. 8 shows that the lithium ion diffusion coefficient has an Arrhenius-type temperature dependence over the whole temperature range. From the slope and intercept of the curve, the activation energy for lithium ion diffusion, E^*, and diffusivity pre-exponential factors, D_0, can be calculated according to Eq. (8). The simulated values of E^* and D_0

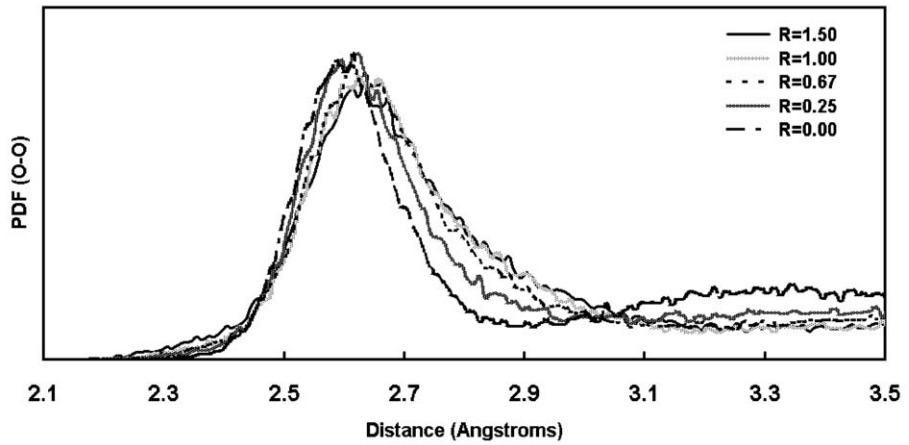

Fig. 5. The first neighbor peaks in the PDF of O–O atom pairs at room temperature.

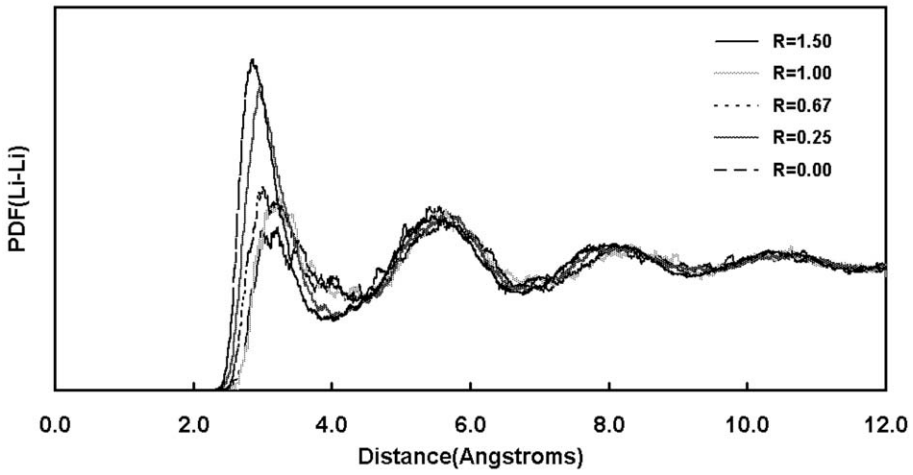

Fig. 6. PDF of Li–Li atom pairs at room temperature.

for all of the glasses are listed in Table 4 and compared with the related experimental values.

Fig. 9 shows the relationship between the activation energy for lithium diffusion and R. For $R=0.00$, i.e. the Li_2SiO_3 glasses, the activation energy is 0.75 eV, which is in good agreement with the experimental result of 0.78 eV observed by Beier and Frischat [10]. In addition, from Fig. 9, the activation energy for lithium diffusion in these glasses decreases to 0.66 eV by altering the concentration of Al. This value of 0.66 eV at $R=1.00$ is similar to the value obtained experimentally in lithium aluminosilicate glasses with an R-value equal to 1.00 (0.68 eV) [14]. Since the pre-exponential (D_0) is quite close for the $R=0.00$ and $R=1.00$ systems (0.0019 cm^2/s versus 0.0014 cm^2/s, respectively, see Table 4), the lower activation energy implies more rapid diffusion in these glasses with $R=1.00$.

These results are similar to the behavior seen in sodium aluminosilicate glasses. Previous simulations have shown that the activation energy for sodium diffusion in sodium aluminosilicate glasses also reaches minimum when [Al]/[Na] = 1.00 [15,16], consistent with experimental behavior observed in these systems [17–20].

The relationship between lithium ion activation energy for diffusion and the composition in the simulated lithium aluminosilicate glasses shows a curve similar to that between sodium activation energy for diffusion and the composition in sodium aluminosilicate glasses [15,16]. Similar interpretations can be made to explain the relationship between lithium ion activation energy for diffusion and the composition in lithium aluminosilicate glasses. Since the interpretation of the change in Na diffusion as a function of composition has been previously discussed, only a brief summary is presented here.

A model for lithium ion transport in a lithium aluminosilicate glasses is that the modified continuous random networks of $[SiO_4]$ and $[AlO_4]$ tetrahedra form a three-dimensional network of available sites for the hopping of lithium ions. When $R<1.00$, lithium ions are predominantly

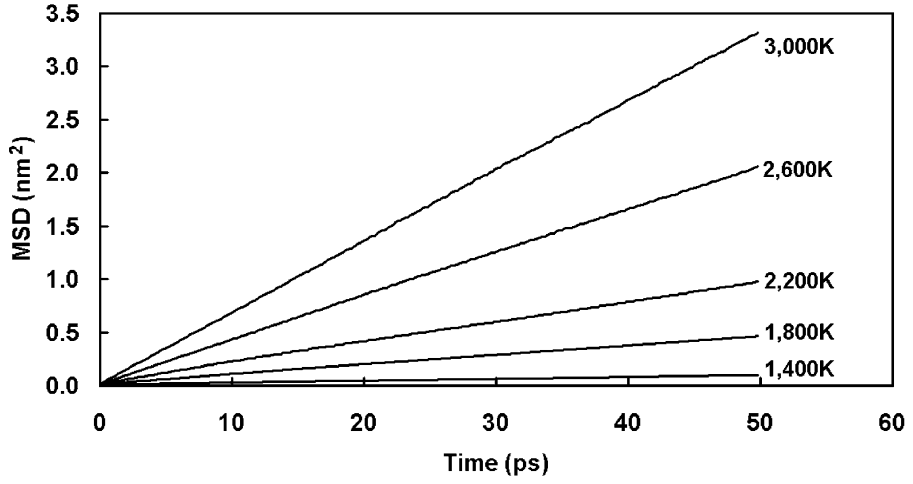

Fig. 7. Mean squared displacement (MSD) of Li ions in glass with $R=0.25$ at different temperatures.

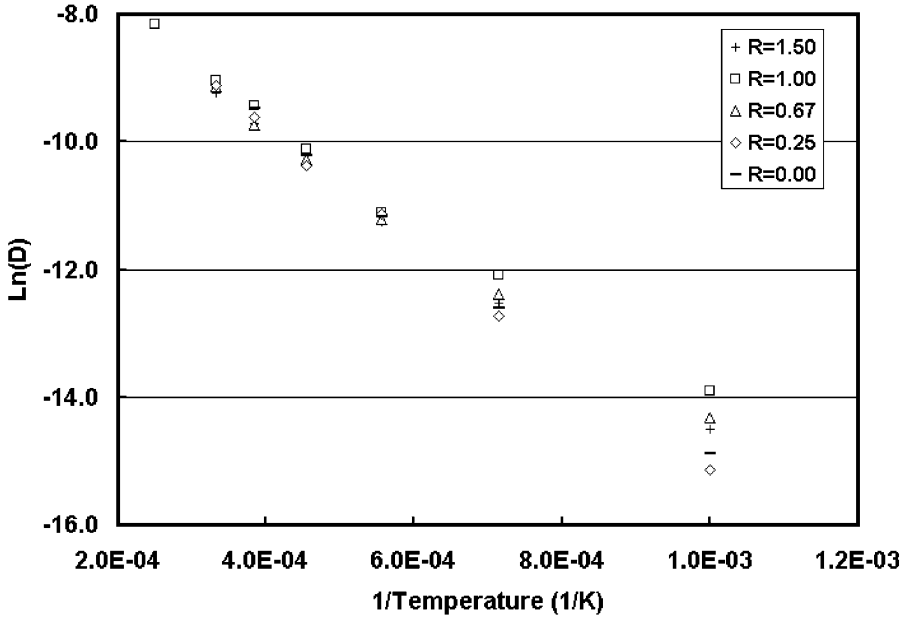

Fig. 8. Li ions diffusion coefficient (D) at different temperatures. (The unit of D is cm^2/s).

bonded to NBO. Diffusion of the lithium ions occurs as Li–NBO bonds are broken and lithium ions hop between NBO sites. The activation energy for diffusion is high for compositions with $R<1.00$ as it is difficult to break the Li–NBO bonds. With the increase of the concentration of Al ions, there are fewer NBOs in the system and more lithium ions are associated with bridging oxygens. Since the X–NBO bond length is slightly smaller and the binding energy is stronger than the X–BO bond (X = Na, Li), the activation energy for lithium diffusion is decreased when the lithium ion is more weakly bound to the BO than to an NBO. When $R=1.00$, there are nearly no Li–NBO bonds. The activation energy in glass with $R=1.00$ is the smallest in the simulated glasses. The initial increase in activation energy is caused by the $(AlO)_4^-$ sites that block channels for lithium diffusion between NBO sites. That is, the channel structure in the modified random network structure of the glasses is closed by the presence of Al ions [10]. When $R>1.00$, lithium ions are predominantly bonded to the $(AlO)_4^-$ anion. However, the activation energy at $R=1.50$ is higher than that at $R=1.00$. It is attributed to the presence of triclusters (oxygens that are bonded to three cations) and the elimination of the large NBO-lined channels, which increase the diffusion distance of lithium ions to find favorable sites, therefore, increasing the activation energy [15]. Triclusters are arguably present in aluminosilicate glasses [34] and would be expected to form in regions of excess Al, as in the case of $R=1.50$.

Table 4
The values of the activation energy for lithium ion diffusion, E^*, and diffusivity pre-exponential factors, D_0, in simulated glasses

R-value	Diffusivity pre-exponential factors D_0 (10^{-3} cm^2/s)	Activation energy E^*(eV) [ref]	
		Simulated	Experimental
1.50	1.2	0.68	
1.00	1.4	0.66	0.68 [14]
0.67	1.2	0.67	
0.25	2.1	0.78	
0.00	1.9	0.75	0.78 [10]

Enhancing Li diffusion through a solid electrolyte used in thin film electrochromic devices or batteries is important and the presence of Al in the glass would enable this. However, Garcia and Garofalini [35] found that there is a buildup of lithium ions at the interface between a Li_2SiO_3 glass electrolyte and the layered V_2O_5 crystal cathode with the (001) planes parallel to the interface. Their work showed that the potential energy for lithium at the interface is lower than that in the glasses (but, of course, not as low as Li within the vanadia cathode itself). This difference in potential enables lithium ion diffusion from the glass to the cathode crystal. (Of course, the actual driving force in a real system is the potential difference between the anode and the cathode.) However, the activation barrier for Li migration across the (001) planes, in the ⟨001⟩ direction, is very high and causes the buildup of Li ions at the interface [35], as shown in Fig. 10a (which is taken from Ref. [35]). In this figure, the bottom of each image is the electrolyte glass (a lithium metasilicate) and the top of each image is the vanadia crystal in two different orientations. The images indicate that the structure of the cathode at the interface may be more important than altering the composition of the glassy electrolyte on improving the response time and conductivity in thin film solid state electrochemical devices. Li diffusion in the ⟨010⟩ direction in the vanadia crystal has a low activation barrier (~ 0.8 eV) [35]. Therefore, the

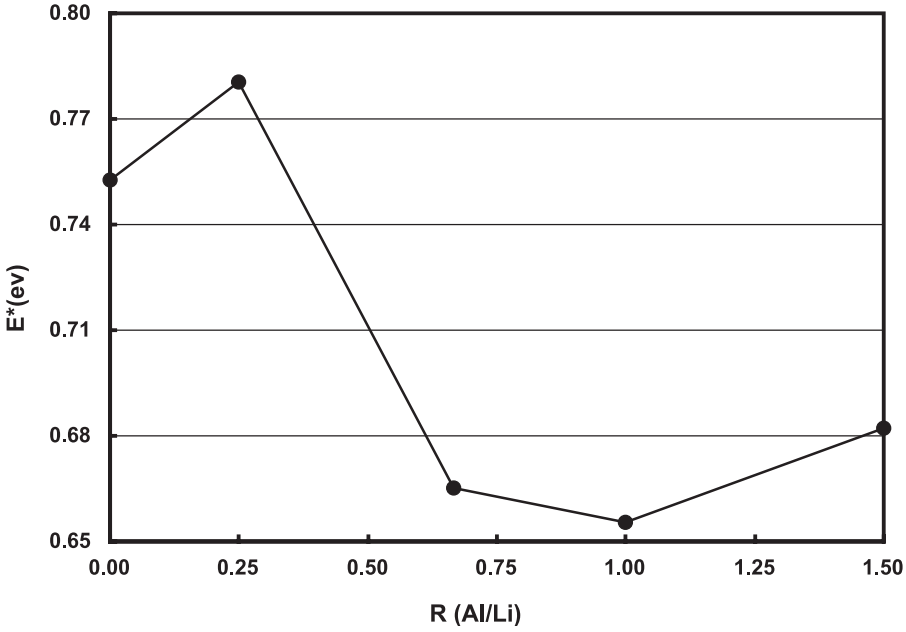

Fig. 9. Activation energy (E^*) of Li ions diffusion as a function of glass composition. Line is only used to show the variation of data points.

system would benefit with the vanadia crystal oriented at the interface with the planes perpendicular to the crystal/glass interface (the ⟨010⟩ direction of the crystal parallel to the surface normal, as in Fig. 10b). However, scanning probe microscopy of an in situ deposited 30 nm film of vanadia cathode over an oxide glass electrolyte showed that the orientation of this layered crystalline cathode has the ⟨001⟩ direction parallel to the surface normal (equivalent to Fig. 10a) [36]. Hence, since nature predisposes this deposited layered system to have the wrong orientation at the interface for the most rapid transport of Li ions from the glass to the cathode, engineering the design of the cathode at the

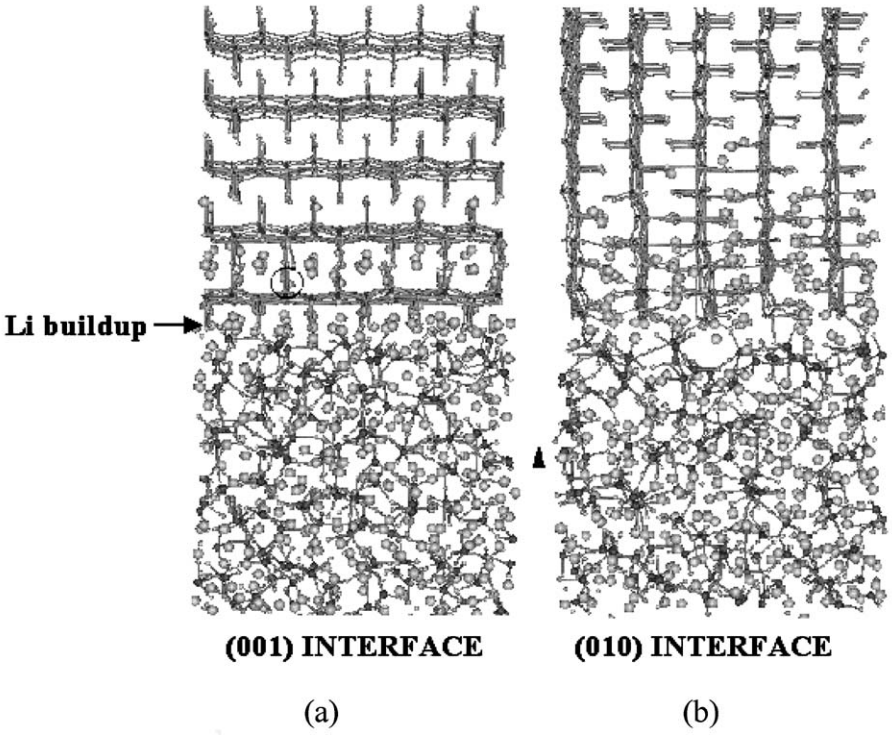

Fig. 10. Two orientations of layered vanadia (top) on lithium metasilicate glass electrolyte (bottom) showing buildup of Li ions in the (a) (001) interface orientation versus migration into the crystal in the (b) (010) orientation. Large spheres are Li ions. From Ref. [35].

interface may be more important than enhanced Li diffusion in the thin film solid electrolyte.

4. Conclusions

The Molecular Dynamics simulation technique was used to model lithium aluminosilicate glasses. The local structure in the glasses compared favorably with the experimentally derived structural features of lithium aluminosilicate glasses. Lithium ion diffusion coefficients at different temperatures were calculated and used to calculate the activation energy of lithium ions in a series of lithium aluminosilicate glasses. The calculated activation energy of lithium ions at the [Al]/[Li] ratio, R, equal to 0.00 was 0.75 eV, in good agreement with Beier and Frischat's experimental result of 0.78 eV [10]; with $R = 1.00$, the simulated value was 0.66 eV, in good agreement with the experimental value of 0.68 eV obtained by Johnson et al. [14]. The minimum in the activation energy for lithium diffusion is exhibited at $R = 1.00$ in the simulated glasses, similar to experimentally observed behavior in sodium aluminosilicate glasses.

Acknowledgements

The authors would like to acknowledge support from the DOE, OBES, Division of Chemical Sciences, Geosciences, Biosciences, Grant Number DE-FGO2-93ER14385.

References

[1] C.-H. Lee, K.H. Joo, J.H. Kim, S.G. Woo, H.-J. Sohn, T. Kang, Y. Oh, J.Y. Oh, Solid State Ionics 149 (2002) 59–65.
[2] K. Takada, S. Kondo, Ionics 4 (1998) 42–47.
[3] K. Takada, N. Aotani, K. Iwamoto, S. Kondo, Solid State Ionics 79 (1995) 284–287.
[4] D.A. Hensley, S.H. Garofalini, Solid State Ionics 82 (1995) 67–73.
[5] J.B. Bates, N.J. Dudney, G.R. Gruzalski, R.A. Zuhr, A. Choudhury, C.F. Luck, J.D. Robertson, J. Power Sources 43/44 (1993) 103–110.
[6] A. Pechenik, D.H. Whitmore, J. Non-Cryst. Solids 101 (1988) 54–56.
[7] A. Pechenik, S. Susman, D.H. Whitmore, M.A. Ratner, Solid State Ionics 18–19 (1986) 403–409.
[8] M. Guedes, A.C. Ferro, J.M.F. Ferreira, J. Eur. Ceram. Soc. 21 (2001) 1187–1194.
[9] C.J. Leo, B.V.R. Chowdari, G.V. Subba Rao, J.L. Souquet, Mater. Res. Bull. 37 (2002) 1419–1430.
[10] W. Beier, G.H. Frischat, J. Non-Cryst. Solids 38 & 39 (1980) 569–573.
[11] B. Wang, S. Szu, M. Greenblatt, L.C. Klein, Chem. Mater. 4 (1992) 191–197.
[12] K. Radhakrishnan, B.V.R. Chowdari, Solid State Ionics 51 (1992) 197–202.
[13] O. Kanert, R. Küchler, D. Suter, G.N. Shannon, H. Jain, J. Non-Cryst. Solids 274 (2000) 202–207.
[14] R.T. Johnson, R.M. Biefeld, M.L. Knotek, B. Morosin, J. Electrochem. Soc. 123 (1976) 680–687.
[15] D.M. Zirl, S.H. Garofalini, J. Am. Ceram. Soc. 73 (1990) 2848–2856.
[16] A.N. Cormack, J. Non-Cryst. Solids 232–234 (1998) 188–197.
[17] J.O. Isard, J. Soc. Glass Technol. 43 (1959) 113–123.
[18] E.L. Williams, R.W. Heckman, Phys. Chem. Glasses 5 (1964) 166–171.
[19] R. Terai, Phys. Chem. Glasses 10 (1969) 146–152.
[20] H. Wakabayashi, Phys. Chem. Glasses 30 (1989) 51–54.
[21] S.H. Garofalini, H. Melman, Application of molecular dynamics simulations to sol–gel processing, in: Better Ceramics Through Chemistry II, vol. 73, Materials Research Society, Aneheim, 1986, pp. 497–505.
[22] A. Rosenthal, S.H. Garofalini, J. Am. Ceram. Soc. 70 (1987) 821.
[23] B.P. Feuston, S.H. Garofalini, J. Chem. Phys. 89 (1988) 5818–5824.
[24] B.F. Feuston, S.H. Garofalini, J. Phys. Chem. 94 (1990) 5351–5356.
[25] S.H. Garofalini, J. Non-Cryst. Solids 120 (1990) 1–12.
[26] S.H. Garofalini, G. Martin, J. Phys. Chem. 98 (1994) 1311–1316.
[27] S. Blonski, S.H. Garofalini, Surf. Sci. 295 (1993) 263–274.
[28] M. Garcia, E. Webb, S.H. Garofalini, J. Electrochem. Soc. 145 (1998) 2155–2164.
[29] J. Zhao, P.H. Gaskell, M.M. Cluckie, A.K. Soper, J. Non-Cryst. Solids 232–234 (1998) 721–727.
[30] S. Sen, T. Mukerji, J. Non-Cryst. Solids 293–295 (2001) 268–278.
[31] G.N. Greaves, A. Fontaine, P. Lagarde, D. Raoux, S.J. Gurman, Nature 293 (1981) 611–616.
[32] G.N. Greaves, J. Non-Crys. Solids 71 (1985) 203–217.
[33] K.L. Geisinger, G.V. Gibbs, A. Navrotsky, Phys. Chem. Miner. 11 (1985) 266–283.
[34] M. Schmucker, H. Schneider, J. Non-Cryst. Solids 311 (2002) 211–215.
[35] M. Garcia, S.H. Garofalini, J. Electrochem. Soc. 146 (1999) 840–849.
[36] A.E. Semenov, I.N. Borodina, S.H. Garofalini, J. Electrochem. Soc. 148 (2001) A1239–A1246.
[37] O.V. Mazurin, M.V. Streltsina, T.P. Shvaiko-Shvaikovskaya, Handbook of Glass Data: Part C. Ternary silicate glasses, Elsevier, New York, 1983.